

# Frequency-swept ultrasound-modulated optical tomography in biological tissue by use of parallel detection

Gang Yao, Shuliang Jiao, and Lihong V. Wang

Optical Imaging Laboratory, Biomedical Engineering Program, Texas A&M University, 3120 TAMU, College Station, Texas 77843-3120

Received January 7, 2000

A frequency-swept ultrasonic beam was focused into a biological tissue sample to modulate the laser light passing through the ultrasonic beam inside the tissue. Parallel detection of the speckle field formed by the transmitted laser light was implemented with the source-synchronous-illumination lock-in technique to improve the signal-to-noise ratio. The ultrasound-modulated laser light reflects the local optical and mechanical properties in the ultrasonic beam and can be used for tomographic imaging of the tissue. Sweeping the ultrasonic frequency provides spatial resolution along the ultrasonic axis, which is scalable with the frequency span of the sweep. Two-dimensional images of biological tissue with buried objects were successfully obtained experimentally. © 2000 Optical Society of America

OCIS codes: 170.3880, 120.6150, 110.7050, 110.7170.

A number of optical imaging techniques<sup>1</sup> have been studied for imaging in biological tissues. The key challenge is to overcome the strong scattering of light in biological tissues. Besides purely optical imaging techniques, combinations of optical and ultrasonic techniques have also been explored because ultrasonic waves scatter much less in biological tissues than do optical waves and can directly furnish localization information for imaging. The ultrasound-modulated optical technique<sup>2-5</sup> is one of these hybrid methods. Marks *et al.*<sup>2</sup> investigated the possibility of tagging light with ultrasound. Wang *et al.*<sup>3</sup> developed ultrasound-modulated optical tomography and obtained images in tissue-simulating phantoms. Leveque *et al.*<sup>6</sup> developed a parallel speckle detection scheme that uses a source-synchronized lock-in technique in which a CCD camera works as a detector array. The signal-to-noise ratio (SNR) can be greatly improved by averaging of the signals from all the CCD pixels. This new technology allowed Leveque *et al.* to obtain one-dimensional (1D) images of buried objects in biological tissue. Recently Yao and Wang<sup>7</sup> obtained two-dimensional (2D) images of multiple objects buried in biological tissues by using this technique. They also demonstrated that ultrasound-modulated diffuse light is useful for imaging, although it has been shown that diffuse light can be modulated by ultrasound without forming images.<sup>8</sup> However, the spatial resolution along the ultrasonic axis is not good in densely scattering biological tissue because the imaging signal consists of contributions from a relatively long zone.

Wang and Ku<sup>9</sup> developed a technique called frequency-swept ultrasound-modulated optical tomography to achieve controllable spatial resolution along the ultrasonic axis. In their experiment, one frequency-sweep function (chirp) excited the ultrasonic transducer while another chirp modulated the gain of the optical detector. When the heterodyne signal from the optical detector was Fourier transformed, the signal from a specific spatial location was converted into a specific frequency component. However, because

of the limited SNR of the single-detector scheme, this technique was demonstrated only for ballistic imaging.

We have extended the frequency-swept modulation technique<sup>9</sup> in the present study, using parallel detection.<sup>6</sup> The laser and the ultrasonic transducer were both modulated with chirp functions. We obtained imaging along the ultrasonic axis by electronically scanning the time delay between these two functions. 2D images of biological tissues with buried objects were obtained with spatial resolution of 4 mm along the ultrasonic axis. We demonstrated that this technique was not dependent on purely ballistic photons by using an obliquely incident laser beam. The scalability of the spatial resolution along the acoustic axis with this technology was also studied.

The experimental setup is shown in Fig. 1. A coordinate system was set up for reference. The Z axis was along the optical axis pointing to the CCD camera. The Y axis was on the acoustic axis pointing from the ultrasonic transducer to the sample. The X axis was perpendicular to both the acoustic and the optical axes. Ultrasonic waves were generated by a focused ultrasonic transducer (Panametrics, V314) with a 2.54-cm focal length in water and a 1-MHz central response frequency. The peak pressure at the focus was  $\sim 2 \times 10^5$  Pa, well below the damage threshold for biological tissues.<sup>10</sup> The laser beam from a diode laser

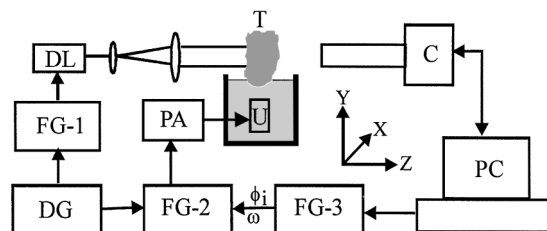


Fig. 1. Schematic of the experimental setup: DL, diode laser; C, CCD camera; U, ultrasonic transducer; PA, power amplifier; T, tissue sample; other abbreviations defined in text.

(Melles Griot 56IMS667, 690-nm wavelength) was expanded to  $1.6 \text{ cm} \times 0.3 \text{ cm}$ , matching the shape of the ultrasonic column, and projected directly onto the tissue sample. The average power of the modulated laser beam was 12 mW. The coherence length was  $\sim 7 \text{ cm}$ . The tissue sample was partially immersed in water for good acoustic coupling. The light transmitted through the tissue sample generated a speckle pattern, which was detected by a high-speed digital CCD camera (Dalsa CA-D1-0256T). Three function generators (Stanford Research Systems DS345), FG-1–FG-3, shared the same time base to ensure synchronization. FG-1 and FG-2 generated chirp functions to modulate the diode laser and to excite the ultrasonic transducer, respectively. A delay–pulse generator, DG, controlled the time delay between the trigger signals to FG-1 and FG-2. If the signal from FG-2 were not amplitude modulated by FG-3, the frequency of the heterodyne signal from location  $y$  along the ultrasonic axis ( $Y$  axis) would be<sup>9</sup>

$$f(y, \tau) = b[\tau - (y/v_s)], \quad (1)$$

where  $b$  is the frequency sweep rate,  $v_s$  is the ultrasonic velocity, and  $\tau$  is the time delay between the two chirps from FG-2 and FG-1. To implement the source-synchronized lock-in technique we used FG-3 to produce a sinusoidal wave with a frequency equal to  $f(y, \tau)$ , which modulated the amplitude of the chirp function generated by FG-2. The signal in a single CCD pixel can be represented as<sup>7</sup>

$$I_i \propto I_b + I_m \cos(\phi + \phi_i), \quad (2)$$

where  $I_b$  is the background intensity,  $I_m$  is the signal intensity related to the ultrasound-modulated component,  $\phi$  is the randomly distributed initial phase of the speckle, and  $\phi_i$  is the initial phase of the sinusoidal wave from FG-3. The quantity  $M = I_m/I_b$  is related to the modulation depth, which reflects the local optical and ultrasonic properties. The initial phase  $\phi_i$  of this sinusoidal wave was set sequentially to  $0^\circ$ ,  $90^\circ$ ,  $180^\circ$ , and  $270^\circ$ . We acquired the corresponding four frames of CCD images to calculate  $M$  as follows:

$$M = (1/2I_b)[(I_{90^\circ} - I_{270^\circ})^2 + (I_{0^\circ} - I_{180^\circ})^2]^{1/2}. \quad (3)$$

The above calculation was performed for each pixel of the CCD camera. A total of  $256 \times 256$ -pixel data were then averaged to produce a single data point for the image. We averaged 50 such measurements to improve the SNR further.

In the experiments, time delay  $\tau$  was scanned while the lock-in frequency from FG-3 was set to a fixed value  $f_0$ . From Eq. (1), the ultrasound-modulated light from a specific spatial location  $y_0$  corresponding to the heterodyne frequency  $f_0$  was detected. The ultrasound-modulated light from the other spatial locations had different frequencies and hence was rejected by the CCD camera. We obtained 1D images along the ul-

trasonic axis by electronically scanning time delay  $\tau$ . To obtain 2D tomographic images we mechanically scanned the ultrasonic transducer with a translation stage along the  $X$  axis.

The tissue samples used in the experiments were skinless chicken-breast tissues bought from a supermarket. The objects buried in the tissue were made from soft rubber, which has good acoustic coupling with tissue and has little acoustic absorption. Figure 2 shows a 2D image obtained from 1.2-cm-thick chicken-breast tissue with a buried object. The size of the object was  $4.0 \text{ mm} \times 2.7 \text{ mm} \times 6.2 \text{ mm}$  along the  $X$ ,  $Y$ , and  $Z$  axes, respectively. The step size of the electronic scan along the  $Y$  axis was  $1.0 \mu\text{s}$ , corresponding to 1.58 mm in the tissue. The step size of the mechanical scan along the  $X$  axis was 1.5 mm. Our experiments indicated that the modulated signal intensity had small variations along the ultrasonic axis, which were caused by the small detection area ( $4 \text{ mm} \times 4 \text{ mm}$ ) of the CCD camera and the ultrasonic pressure distribution along the ultrasonic axis. To compensate for this variation we normalized the raw 1D images along the  $Y$  axis by the result obtained from uniform-background tissue. In the image shown in Fig. 2 the buried object is clearly visible in the background. The image resolution along the  $X$  axis is  $\sim 2 \text{ mm}$ , which is determined by the 2-mm focal diameter of the ultrasonic transducer used in the experiments. The spatial resolution along the ultrasonic axis ( $Y$  axis)  $\Delta y$  is determined by the frequency span  $\Delta f$  of the chirp function and the ultrasonic velocity  $v_s$  as follows:  $\Delta y \approx v_s/\Delta f$ .<sup>9</sup> In the experiments,  $v_s \approx 1580 \text{ m/s}$  and  $\Delta f = 400 \text{ kHz}$ , which yields  $\Delta y \approx 4 \text{ mm}$ . One can scale the spatial resolution along the ultrasonic axis by changing the frequency span  $\Delta f$ . To demonstrate this scalability we acquired two 1D images with frequency spans  $\Delta f = 400 \text{ kHz}$  and  $\Delta f = 800 \text{ kHz}$ , corresponding to spatial resolutions of 4 and 2 mm, respectively [Fig. 3(a)]. The buried object had a thickness of 3 mm along the  $Y$  axis. As shown in the results, the 1D image obtained with  $\Delta f = 800 \text{ kHz}$  has sharper edges than the image obtained with  $\Delta f = 400 \text{ kHz}$ . However, the intensity of the signal with the better spatial resolution is less because the spatial volume that contributes to the signal is reduced.

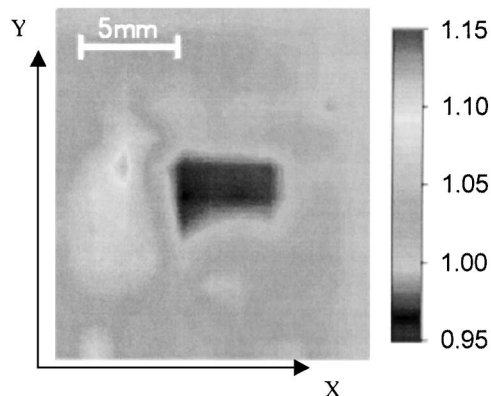


Fig. 2. Experimental 2D image of 1.2-cm-thick chicken-breast tissue containing a buried object.

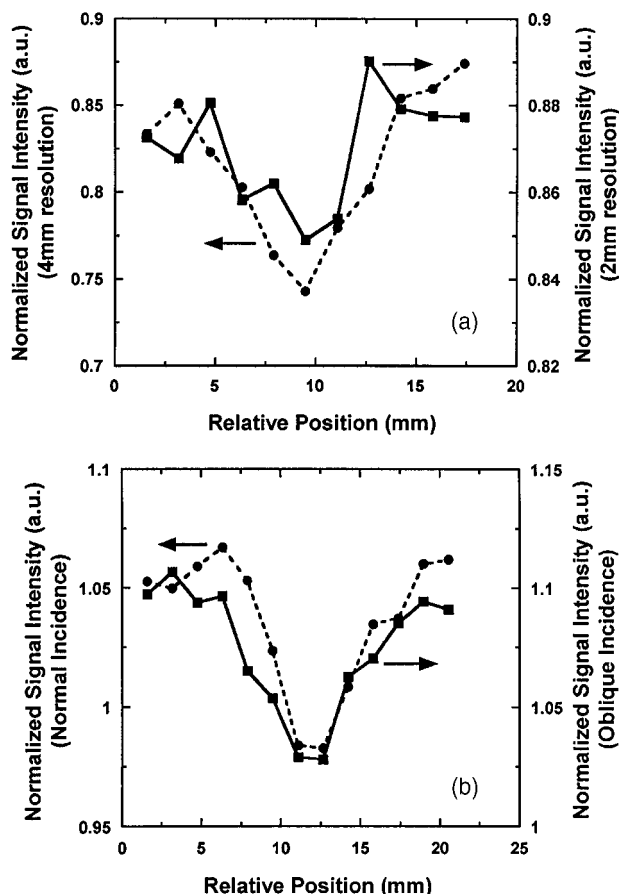


Fig. 3. (a) 1D images of 1.2-cm-thick chicken-breast tissue with spatial resolutions of 4 and 2 mm along the ultrasonic axis. (b) 1D images of 1.2-cm-thick chicken-breast tissue with a normally incident laser beam and an obliquely incident laser beam at  $10^\circ$ .

The absorption coefficient of the chicken-breast tissue is  $\sim 0.1 \text{ cm}^{-1}$ , and the reduced scattering coefficient is  $\sim 2 \text{ cm}^{-1}$  at  $\sim 700 \text{ nm}$ .<sup>11</sup> Ballistic photons are expected to be weak, if detectable at all, after transmitting the 1.2-cm-thick chicken-breast tissue. To further eliminate the possibility of collecting purely ballistic imaging photons, we acquired a 1D ultrasound-modulated optical image with the laser beam illuminating the sample obliquely at  $10^\circ$  to the  $Z$  axis. Any ballistic photons, if they existed, would have missed the detector. The signal intensity ( $M$ ) measured in the case of oblique incidence was almost the same as that measured in the case of normal incidence. As shown in Fig. 3(b), there is no significant difference between the two images. From this result it is clear that purely ballistic photons are not the major contributors to the signal in our experiments and that ultrasound-modulated optical tomography depends mainly on diffuse light.

As the modulated signal intensity is usually quite small compared with the unmodulated background signal, the SNR is critical in ultrasound-modulated optical tomography. The image contrast is also directly related to SNR. Shot noise is the major noise contributor in the experiments. To maintain a high enough SNR, the CCD camera needs to receive enough photons by using a long exposure time. In our experiments the single-frame exposure time was  $\sim 150 \text{ ms}$ . However, besides slowing down the data acquisition, the long exposure time may cause the SNR to suffer from decorrelation of the speckle field. Obviously one could overcome this problem by simply increasing the incident laser power. The average power density in our experiments is  $\sim 25 \text{ mW/cm}^2$ , which can be raised to  $\sim 200 \text{ mW/cm}^2$ , limited by the American National Standards Institute standards for 690-nm laser light. In addition, the SNR could also be improved by use of a detector with a higher dynamic range because the signal is currently extremely small compared with the background.

In conclusion, by combining the frequency-swept ultrasound-modulation technique with the parallel-detection scheme, we obtained 2D images of 1.2-cm-thick chicken-breast tissue containing buried objects and achieved spatial resolution of  $\sim 4 \text{ mm}$  along the ultrasonic axis. The lateral spatial resolution was  $\sim 2 \text{ mm}$  and was determined by the focal width of the ultrasonic transducer. This technique can be directly applied to acquiring three-dimensional images in turbid media.

This project was sponsored in part by National Institutes of Health grants R29 CA68562, R01 CA71980, and R21 CA83760 and by National Science Foundation grant BES-9734491. L. Wang's e-mail address is lwang@tamu.edu.

## References

1. J. G. Fujimoto and M. S. Patterson, eds., *Advances in Optical Imaging and Photon Migration*, Vol. 2 of OSA Trends in Optics and Photonics Series (Optical Society of America, Washington, D.C., 1998).
2. F. A. Marks, H. W. Tomlinson, and G. W. Brooksby, *Proc. SPIE* **1888**, 500 (1993).
3. L.-H. Wang, S. L. Jacques, and X. Zhao, *Opt. Lett.* **20**, 629 (1995).
4. L.-H. Wang and X. Zhao, *Appl. Opt.* **36**, 7277 (1997).
5. M. Kempe, M. Larionov, D. Zaslavsky, and A. Z. Genack, *J. Opt. Soc. Am.* **14**, 1151 (1997).
6. S. Leveque, A. C. Boccara, M. Lebec, and H. Saint-Jalmes, *Opt. Lett.* **24**, 181 (1999).
7. G. Yao and L.-H. Wang, *Appl. Opt.* **39**, 659 (2000).
8. W. Leutz and G. Maret, *Physica B* **204**, 14 (1995).
9. L.-H. Wang and G. Ku, *Opt. Lett.* **23**, 975 (1998).
10. T. A. Whittingham, *Imaging* **6**, 33 (1994).
11. G. Marquez, L.-H. Wang, S.-P. Lin, J. A. Schwartz, and S. L. Thomsen, *Appl. Opt.* **37**, 798 (1998).